

Accurate Analysis of JEM Interference in Airborne Array using Parallel HO-IE-DDM

Yingyu Liu¹, Qin Su¹, Xunwang Zhao¹, Yu Zhang¹, Zhongchao Lin¹, Chang Zhai¹,
and Qi Zhang²

¹ Shaanxi Key Laboratory of Large Scale Electromagnetic Computing
Xidian University, Xi'an, Shaanxi 710071, China
xwzhao@mail.xidian.edu.cn

² Science and Technology on Electromagnetic Compatibility Laboratory
China Ship Development and Design Center, Wuhan 430064, China

Abstract — In this paper, we present a parallel integral equation solver based on domain decomposition method for the analysis of airborne array interference problems affected by jet engine modulation. The solver makes use of higher-order basis functions for the discretization of the problem. The paper proposes two main novelties: firstly, the radiation characteristics of the airborne array (interfered by multiple rotating blades) are analyzed using an integrated simulation technology; secondly, the computation during the analysis of JEM problem is significantly reduced, for only re-computing the changed parts of the model. Numerical examples using complex electrically large structures are presented in order to demonstrate the flexibility, accuracy, and efficiency of the proposed integral equation solver.

Index Terms — Airborne antenna array, domain decomposition method, higher-order MoM, Jet engine modulation, parallel.

I. INTRODUCTION

Radar is regarded as a powerful tool for detecting and tracking airborne targets. For a radar system, the antenna pattern provides input information. However, due to the nearfield scattering from the platform, the antenna radiation pattern can be distorted. This distorted pattern may seriously affect the detection performance of the radar [1]. For a common carrier platform, an airplane, there are some rotating parts of it like blades of turbofan engine and propeller-fan engine [1-3]. These rotating objects can cause a periodic modulation of electromagnetic (EM) wave radiated by antenna array, which is known as jet engine modulation (JEM). Thus, this effect can result in a miscomputation of radar prediction.

For a long time, researches about JEM issues are mainly limited in scattering characteristics [1-4]. For

more complex EM problem, the radiation patterns of the antenna affected by JEM effect, it was not until last decade to be carried out [5]. Usually, the antennas involved are simpler structures such as a dipole antenna at lower working frequency, and only one single rotor can be calculated. Due to the large electrical size of the whole targets and the complex EM environment, such electromagnetic compatibility (EMC) problem is extremely challenging. Scholars generally use high frequency algorithm like uniform geometrical theory of diffraction (UTD) [6] and physical optics (PO) to analyze JEM. However, such method fails to ensure sufficient accuracy. Using method of moment (MoM) to study JEM can get accurate results, but MoM usually requires very large computational resources [7].

It could be an effective way to solve the EM problems from electrically large structures combining the method of integral equations (IE) with the domain decomposition method (DDM). There are also some studies on IE-DDM [8-11]. However, they are mostly aimed at solving the scattering problem. Even if the radiating problem can be analyzed, it is difficult to analyze large complex issues such as the airborne antenna array. Let alone the JEM issues of the large airborne antenna arrays. Among these studies on IE-DDM, it is worthwhile to mention the work presented by Peng and Lee [9], which is able to address multi-scale issue with non-conformal meshes. It is possible to only re-mesh the changed portion of a target, but the whole problem still need to be re-computed.

A new solution scheme of integral equations based on domain decomposition method discretized by higher-order basis functions, called as HO-IE-DDM, is proposed in this paper. The advantages of the higher-order basis functions, which are used to approximate the current distribution [7,12,13], are that produce fewer unknowns than lower-order basis functions and increase the scale

of the problem to be solved. By bringing parallel computing technique in the HO-IE-DDM, the simulating capability of the method is further improved. The proposed parallelization scheme allows all the computer resources to be used to a single subdomain at a time, the advantage of which is that the imbalanced workload caused by the unevenly decomposed subdomains is reduced, and at the same time the scale of the problem to be solved is greatly enlarged. Moreover, the proposed solver provides unprecedented flexibility and convenience for analysis of JEM issues, since it is possible to only compute the changed part of the aircraft.

The remaining of this paper is organized as follows. In Section II, the algorithm of the HO-IE-DDM is presented. Section III provides two cases of JEM radiation problem are analyzed using parallel HO-IE-DDM, and the numerical examples to demonstrate the correctness, flexibility and high efficiency of the proposed method. Finally, some conclusions are given in Section IV.

II. THEORY OF HO-IE-DDM

A. Integral equations

Let us consider a finite large complex EM target containing multiple perfect electric conductors (PECs) and dielectric structures in free space. In the i th region ($i=1,2,\dots,n$), the permittivity and the permeability are ε_i and μ_i , and the incident electric and magnetic fields are \mathbf{E}_i^{inc} and \mathbf{H}_i^{inc} , respectively, as shown in Fig. 1 (a). Region 0 is for perfect electric conductors (PECs), in which the electromagnetic field is zero.

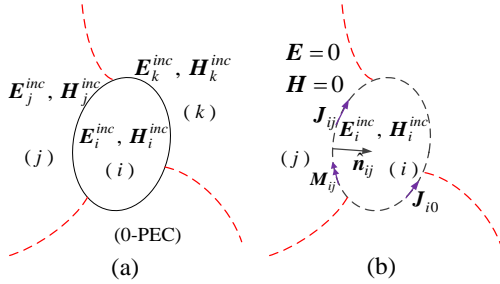


Fig. 1. Surface equivalence theorem: (a) the original problem, and (b) the equivalent problem of region i .

In general, we consider the i th region, as shown in Fig. 1 (b). According to the equivalence principle, the regions except the i th region are filled with the same medium as the i th region. At this time, the electric and magnetic fields in these regions (except the i th region) are $\mathbf{E}=0$ and $\mathbf{H}=0$. The equivalent current density at the boundary surface between region i and j can be expressed as:

$$\mathbf{J}_{ij} = \hat{\mathbf{n}}_{ij} \times \mathbf{H}_i, \mathbf{M}_{ik} = -\hat{\mathbf{n}}_{ij} \times \mathbf{E}_i, \quad (1)$$

where $\hat{\mathbf{n}}_{ij}$ is the unit normal vector. If we consider the

j th region, the equivalent current density at the boundary surface between region j and i can be expressed as:

$$\mathbf{J}_{ji} = \hat{\mathbf{n}}_{ji} \times \mathbf{H}_j, \mathbf{M}_{jk} = -\hat{\mathbf{n}}_{ji} \times \mathbf{E}_j. \quad (2)$$

The electromagnetic field satisfies the following boundary conditions:

$$\hat{\mathbf{n}}_{ij} \times (\mathbf{H}_i - \mathbf{H}_j) = 0, \hat{\mathbf{n}}_{ij} \times (\mathbf{E}_i - \mathbf{E}_j) = 0. \quad (3)$$

Here \mathbf{E}_i and \mathbf{H}_i , the total field in the i th region, are expressed as:

$$\mathbf{E}_i = \sum_{\substack{k=0 \\ k \neq i}}^n [\eta_i L_i(\mathbf{J}_{ik}) - K_i(\mathbf{M}_{ik})] + \mathbf{E}_i^{inc}, \quad (4)$$

$$\mathbf{H}_i = \sum_{\substack{k=0 \\ k \neq i}}^n \left[K_i(\mathbf{J}_{ik}) + \frac{L_i(\mathbf{M}_{ik})}{\eta_i} \right] + \mathbf{H}_i^{inc}, \quad (5)$$

where η_i is the intrinsic impedance of the i th region:

$$L_i(\mathbf{X}_{ik}) = -jk_i \int_{S_{ik}} \left(\mathbf{X}_{ik}(\mathbf{r}_{ik}) G_i(\mathbf{r}, \mathbf{r}') + \frac{1}{k_i^2} \nabla \mathbf{X}_{ik}(\mathbf{r}_{ik}) \nabla G_i(\mathbf{r}, \mathbf{r}') \right) dS_{ik}, \quad (6)$$

$$K_i(\mathbf{X}_{ik}) = -\int_{S_{ik}} (\mathbf{X}_{ik}(\mathbf{r}_{ik}) \times \nabla G_i(\mathbf{r}, \mathbf{r}')) dS_{ik}, \quad (7)$$

where $G_i(\mathbf{r}, \mathbf{r}') = e^{-jk_i R} / 4\pi R$, $R = |\mathbf{r} - \mathbf{r}'|$, $k_i = \omega \sqrt{\varepsilon_i \mu_i}$.

By substituting equations (4) and (5) into equation (3), the surface IE, called the PMCHWT formulation [12], at the boundary surface between region i and j can be obtained by:

$$\hat{\mathbf{n}}_{ij} \times \left\{ \sum_{\substack{k=0 \\ k \neq i}}^n [\eta_i L_i(\mathbf{J}_{ik}) - K_i(\mathbf{M}_{ik})] - \sum_{\substack{k=0 \\ k \neq j}}^n [\eta_j L_j(\mathbf{J}_{jk}) - K_j(\mathbf{M}_{jk})] \right\} = \hat{\mathbf{n}}_{ij} \times (\mathbf{E}_j^{inc} - \mathbf{E}_i^{inc}), \quad (8)$$

$$\hat{\mathbf{n}}_{ij} \times \left\{ \sum_{\substack{k=0 \\ k \neq i}}^n \left[K_i(\mathbf{J}_{ik}) + \frac{L_i(\mathbf{M}_{ik})}{\eta_i} \right] - \sum_{\substack{k=0 \\ k \neq j}}^n \left[K_j(\mathbf{J}_{jk}) + \frac{L_j(\mathbf{M}_{jk})}{\eta_j} \right] \right\} = \hat{\mathbf{n}}_{ij} \times (\mathbf{H}_j^{inc} - \mathbf{H}_i^{inc}). \quad (9)$$

At boundary surfaces between region i and region 0 (PECs), the magnetic currents vanish, so equation (9) is no longer established, and equation (8) degenerates into the electric field integral equation (EFIE) [14].

B. Domain decomposition method

As shown in Fig. 2, the simulation model is decomposed into several subdomains Ω_i ($i=1,2,\dots,n$). Generally, for the n subdomains case, the Galerkin test is performed to the weighted linear combination of equations (8-9) and the following matrix equation is obtained:

$$\begin{bmatrix} \mathbf{Z}_{11} & \mathbf{Z}_{12} & \cdots & \mathbf{Z}_{1n} \\ \mathbf{Z}_{21} & \mathbf{Z}_{22} & \cdots & \mathbf{Z}_{2n} \\ \vdots & \vdots & \ddots & \vdots \\ \mathbf{Z}_{n1} & \mathbf{Z}_{n2} & \cdots & \mathbf{Z}_{nn} \end{bmatrix} \begin{bmatrix} \mathbf{I}_1 \\ \mathbf{I}_2 \\ \vdots \\ \mathbf{I}_n \end{bmatrix} = \begin{bmatrix} \mathbf{V}_1 \\ \mathbf{V}_2 \\ \vdots \\ \mathbf{V}_n \end{bmatrix}, \quad (10)$$

where \mathbf{Z}_{ij} ($i=j$) is the self impedance matrix in Ω_i , \mathbf{Z}_{ij} ($i \neq j$) is the mutual impedance matrix between Ω_j and Ω_i , \mathbf{I}_i is the current coefficient vector in Ω_i and \mathbf{V}_i is the excitation vector in Ω_i .

Parallel out of core higher-order MoM (HOMoM) with the lower/upper decomposition (LU) solver is employed for each part. If the model is decomposed completely evenly, that each subdomain Ω_i contains $M=N/n$ unknowns, the memory requirement and the computing complexity of the LU solver is $O(M^2)$ and $O(M^3)$. If the division is uneven, the memory requirement and the computing complexity depend on the number of unknowns in the largest subdomain.

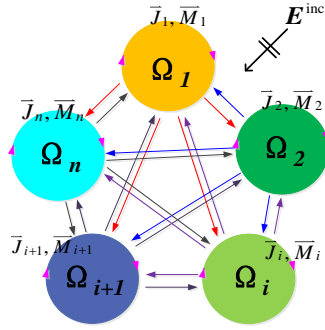


Fig. 2. Notations for domain decomposition.

Noting that the mutual impedance matrices in (10) are unnecessary to be stored, the coupling voltage vector ($\Delta \mathbf{V}_i = \mathbf{Z}_{ij} \mathbf{I}_j$) can be obtained using the near scattered field produced by the current ($\Delta \mathbf{V}_i(\mathbf{E}_{ij}, \mathbf{H}_{ij})$), and hence the memory requirement is reduced. The Gauss–Seidel method is adopted to calculate the interactions among domains allowing the use of all the computer resources in every subdomain problem at a time [15]. The vector of excitation \mathbf{V}_i of Ω_i is updated by other domains at each step:

$$\mathbf{Z}_{ii} \cdot \mathbf{I}_i = \mathbf{V}_i(\mathbf{E}^{\text{inc}}, \mathbf{H}^{\text{inc}}) + \sum_{j=1, j \neq i}^n \Delta \mathbf{V}_i(\mathbf{E}_{ij}, \mathbf{H}_{ij}). \quad (11)$$

Given the tolerance δ , at the initial step $k=0$, $\mathbf{I}_i^{(0)} = 0$ ($i = 1, 2, \dots, n$) and at the $k+1$ th step, the unknown surface current can be expressed as:

$$\mathbf{I}_i^{(k+1)} = \mathbf{Z}_{ii}^{-1} \left[\mathbf{V}_i(\mathbf{E}^{\text{inc}}, \mathbf{H}^{\text{inc}}) + \sum_{j>i} \Delta \mathbf{V}_i(\mathbf{E}_{ij}^{(k)}, \mathbf{H}_{ij}^{(k)}) + \sum_{j<i} \Delta \mathbf{V}_i(\mathbf{E}_{ij}^{(k+1)}, \mathbf{H}_{ij}^{(k+1)}) \right]. \quad (12)$$

The iterative steps continue and the residual error $\varepsilon_i = \|\mathbf{I}_i^{(k+1)} - \mathbf{I}_i^{(k)}\| / \|\mathbf{I}_i^{(k+1)}\|$ is calculated after each step. When $\max(\varepsilon_1, \varepsilon_2, \dots, \varepsilon_n) \leq \delta$ at the k th step, the iterative process stops and outputs \mathbf{I}^k ; otherwise, the process continues. If each subdomain Ω_i contains $M=N/n$

unknowns, the memory requirement and the computing complexity of the iterative process is $O(M)$ and $O(M^2)$. The flowchart of HO-IE-DDM is shown in Fig. 3.

Noting that the inverse matrices of self impedance in (12) is unnecessary to be re-computed, because they have been stored after the initial step. This provides a huge advantage for the analysis of JEM problems. When introducing quasi-stationary method to study how the rotating parts affect the airborne antenna performance, we need to compute the airplane with hundreds of different rotating blades stations. Considering the computing complexity of each subdomain is $O(M^3)$, if we decompose the rotating parts from the main part of the aircraft, the unchanged part can be computed only once. Thus the computing time can be reduced effectively.

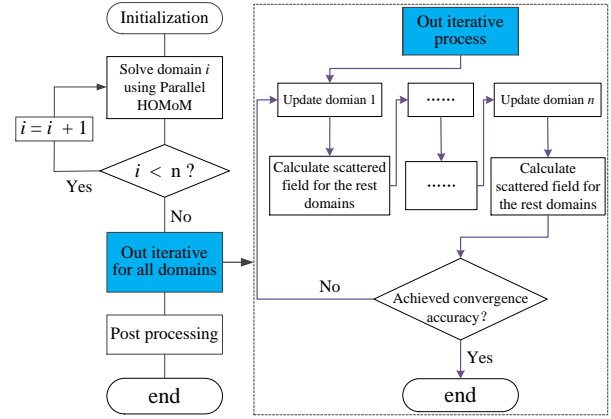


Fig. 3. Flowchart of HO-IE-DDM.

C. High-order basis functions

Different with the traditional RWGs which are defined on triangle patches, the higher-order basis functions (HOBs) employed by the proposed solver are defined on bilinear quadrilateral patches, as shown in Fig. 4. We refer the interested readers to [7,12] for details. The polynomial orders of the HOBs can be adjusted according to the electrical size of the geometric element. The main advantage of HOBs is that the size of the bilinear patch can be much bigger than that of the RWGs [14]. It means that the application of the HOBs can reduce the number of unknowns dramatically.

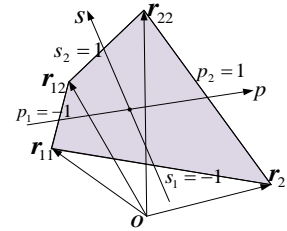


Fig. 4. Bilinear quadrilateral patch.

D. Parallelization

Based on DDM, the computing capability of HOMoM is improved. With the aid of parallel strategy, the computing speed of HO-IE-DDM can be further accelerated. For each subdomain, the large dense MoM matrix is divided into a number of smaller block matrices that are nearly equal in size and distributed among all participating processes. The distribution manner of the blocks is chosen appropriately according to the parallel LU direct solver to minimize the communication between processes.

The LU solver is a numerical accurate method in solving matrix equations, which can solve arbitrary geometric model problems, even if the matrix condition number is bad. For the parallel LU solver, the data should be distributed to multiple processes in a certain way and a load balanced approach called two-dimensional block-cyclic matrix distribution, which is similar to the ScaLAPACK, is adopted. It is important that the matrix filling schemes should be designed to avoid redundant calculation for better parallel efficiency.

Different from other parallel DDM strategy [16], which parallel computation occurs among subdomains, the parallel computation occurs both in and among every subdomains. The parallel strategy will not only simplify the modeling and meshing of subdomains to ensure their unknowns are even, but also save the waiting time to ensure each subdomain has been computed over.

III. COMPUTATIONAL ANALYSIS OF JEM ON AIRBORNE ANTENNA ARRAY

Two EM examples are presented to demonstrate the efficiency and accuracy of the proposed method. The residual error for outer iterative convergence is set to $3.0e-3$ without any specification. Two computational platforms are used in this paper:

Platform I: A workstation with two six-core 64 bit Intel Xeon E5-2620 2.0 GHz CPUs, 64GB RAM and 6TB disk.

Platform II: High-Performance Computing (HPC) cluster with 140 computing nodes. Each computing node has two 12-core bit Intel Xeon E5-2692 2.2 GHz CPUs, 64 GB RAM and 1.8TB disk.

A. Static airborne Yagi-Uda antenna array characteristic

First of all, to validate the accuracy and efficiency of the proposed HO-IE-DDM, the radiation characteristic of an airborne Yagi-Uda antenna array is calculated. The aircraft is $22.03m \times 17.16m \times 6.16m$ [17]. A Yagi-Uda antenna array [18] operated in 500MHz is mounted 2.5m above the middle part of the fuselage. The array consists of 36 units, and each unit has 8 directors. The aircraft model is shown in Fig. 5, which illustrates the relative location of the antenna array. Both sides of the wings are respectively equipped with a rotor. Each blade is

$1.77m \times 0.15m \times 0.03m$. The corresponding electrical size of that is about 2.77λ long, 0.23λ wide, 0.05λ thick. The patterns of antenna array before and after it is mounted on the airplane are shown in Fig. 6.

The model of the aircraft is decomposed into two subdomains as it is shown in Fig. 7. The 2D radiation patterns obtained by the proposed HO-IE-DDM are shown in Fig. 8. The patterns of overall solution using HOMoM and FEKO (a commercial software based on MoM) are also given for comparison.

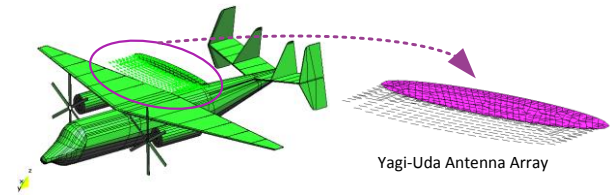


Fig. 5. Model of the double rotor aircraft mounting Yagi-Uda antenna array.

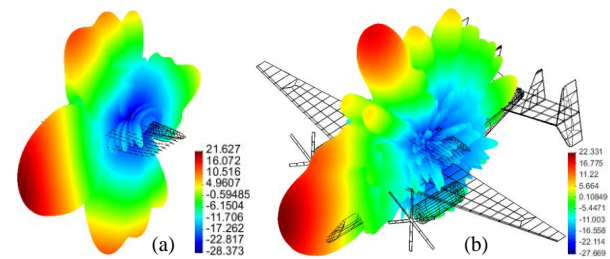


Fig. 6. Yagi-Uda array patterns: (a) array and (b) airborne array.

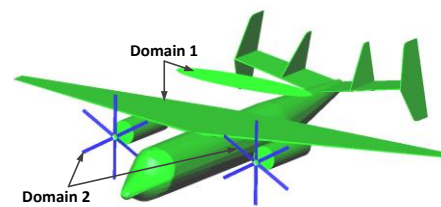


Fig. 7. Domain decomposition model (each color represents a subdomain).

The simulation is performed on Platform I, and the results obtained from HO-IE-DDM and HOMoM agree very well. The results obtained from HO-IE-DDM, HOMoM and FEKO (MoM) also agree well. Some difference between HOMoM and FEKO should result from the different meshes of the triangular meshes for RWGs and the quadrilateral meshes for HOBs. Computing information of radiation characteristics of the model analyzed by parallelized HO-IE-DDM and HOMoM is shown in Table 1. It can be seen that the computing time of HO-IE-DDM is not reduced compared with HOMoM (in core), but reduced compared with

HOMoM (out of core) and FEKO (MoM). For HOMoM (out of core), the computing time is saved owing to the reduction in I/O of hard disk, while for FEKO (MoM), the computing time is saved owing to the reduction in unknowns. We refer the interested readers to [7,8] for details between out of core HOMoM and in core HOMoM.

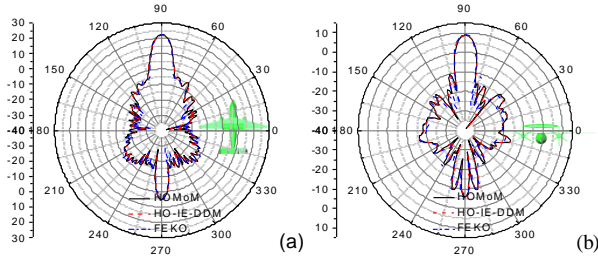


Fig. 8. 2D radiation patterns of the airborne Yagi-Uda array: (a) x-y and (b) x-z.

Table 1: Computational statistics of airborne Yagi-Uda array

| Method | Unknowns | Storage (GB) | Time (s) |
|------------------------|--------------------|--------------------|----------|
| HO-IE-DDM | 30324 (domain1) | 13.70 (domain1) | 1392.6 |
| | 1712 (domain2) | 0.04 (domain2) | |
| HOMoM (out of core) | 31716 | 14.99 | 1424.9 |
| HOMoM (in core) | 31716 | 14.99 | 1283.6 |
| FEKO (MoM) | 126902 | 120.23 | 60439.9 |

B. Dynamic airborne Yagi-Uda antenna array JEM characteristics

Based on quasi-stationary method, 1024 rotor orientations are included in the predictions of 0° to 360° to simulate rotor motion. For each of the fixed rotor orientations, the principal plane radiation pattern is predicted. The level of rotor modulation is calculated for each observation angle. For these comparisons, the level of rotor modulation is defined as the difference between the maximum and minimum magnitudes of the electric field that occur at a given observation angle among the rotor orientations (modulation level = $20\lg|\mathbf{E}_{\max}| - 20\lg|\mathbf{E}_{\min}|$). The accuracy of the proposed method has been proved in Fig. 8.

In order to compare with modulation level, we spread 3D radiation pattern contour plot along θ axis and ϕ axis in Fig. 9. Figure 10 shows the changeable intensity of the airborne array radiation pattern at every observation angles. JEM affects less when the receiving antenna is circularly polarized. Compared with Fig. 9, there is a complementary relationship before and after the

modulation. It shows that side-lobes and null depth levels of the airborne array are intensely changed.

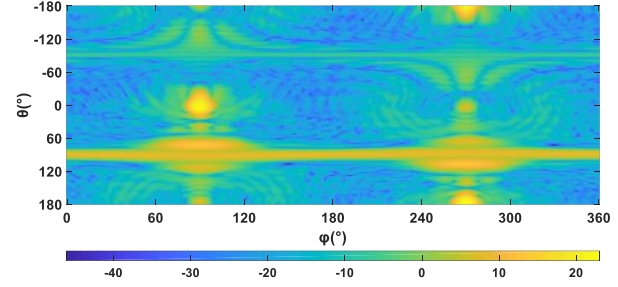


Fig. 9. Spreaded airborne Yagi-Uda array pattern.

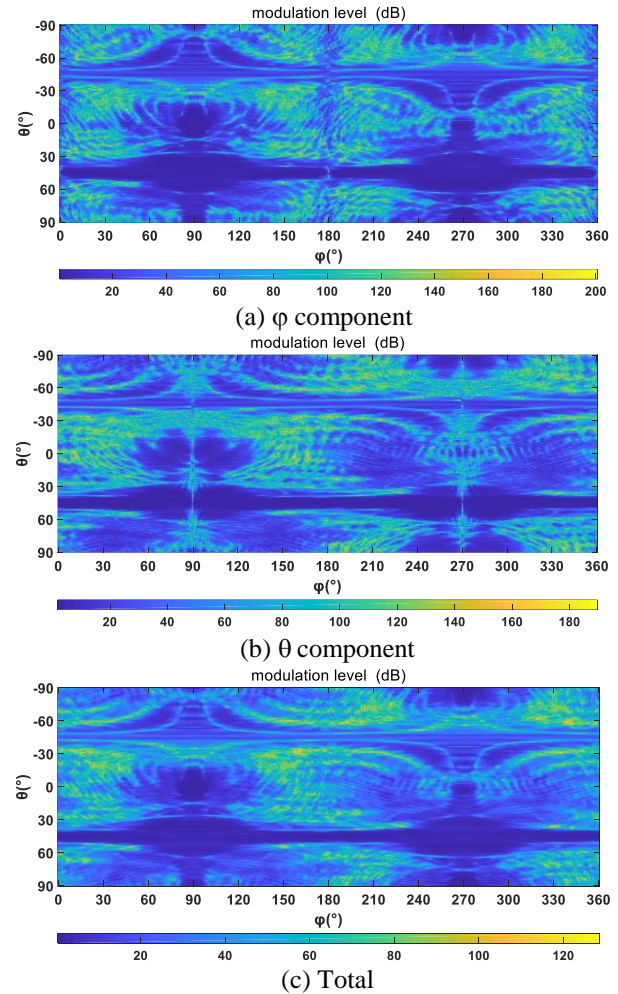


Fig. 10. Spreaded modulation level contour plots.

To save computing time, the modulation level is only computed by HO-IE-DDM. When the turbofans rotate, it needs to perform multiple simulations according to the changed position. For HOMoM (out of core), it needs at least 1024×1424.91 s to simulate the 1024 rotor orientations. As shown in Table 2, when solving the JEM

issues with repetitive similar simulations with changeable parts, HO-IE-DDM exhibits good performance for saving 92% of computation time compared to HOMoM. Because the computation of the main part of an aircraft is only need to do once, and the result of it is stored to be reused in the next 1024 iterations, the computing efficiency is significantly improved.

Table 2: Computational statistics of interfered Yagi-Uda array

| Method | Unknowns | Storage (GB) | Time (s) |
|------------------------|------------------------|------------------------|---|
| HO-IE-DDM | 30324 (domain1) | 13.70 (domain1) | 897.5×1 (domain1) 9.8×1024 (domain2) |
| | 1712×1024 (domain2) | 0.04×1024 (domain2) | 113542.7 (total) |
| HOMoM (out of core) | 31716×1024 | 14.99×1024 | - |

C. Static airborne microstrip antenna array characteristics

Consider a rectangle patch microstrip array with 37×9 elements as shown in Fig. 11. The dimension of the dielectric substrate of a unit is $321.4\text{mm} \times 321.4\text{mm}$, and the dimension of the rectangle patch of a unit is $205.6\text{mm} \times 154.8\text{mm}$. The units are connected with each other. The thickness of the dielectric substrate is 18mm and $\epsilon_r=4.5$, the operating frequency is 700MHz . And the aircraft is $38.6\text{m} \times 36.5\text{m} \times 6.14\text{m}$ [8]. The array [14] is mounted 6.0m above the middle of the fuselage. The aircraft model is shown in Fig. 12, which illustrates the relative location of the antenna array. Both sides of the wings are respectively equipped with two rotors. Each blade is $1.5\text{m} \times 0.3\text{m} \times 0.05\text{m}$. The corresponding electrical size of that is about 2.25λ long, 0.51λ wide, 0.08λ thick. The patterns of antenna array before and after it is mounted on the airplane are shown in Fig. 13.

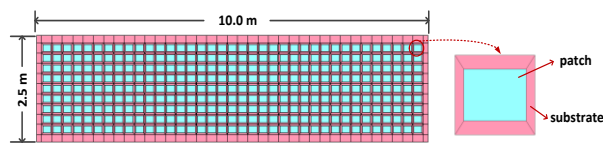


Fig. 11. Model of the microstrip antenna array.

The model is decomposed into four subdomains in this example, and the array is in an independent subdomain. The domain decomposition model of the aircraft for HO-IE-DDM is shown in Fig. 14. The simulation is performed on Platform II and 96 CPU cores are used in this example. The radiation patterns of the airborne antenna array obtained by HO-IE-DDM and the overall solution by HOMoM (out of core) are shown in Fig. 15. They are in good agreement with each other. The

overall solution can neither be obtained by HOMoM (in core) due to the limited computer memory, nor be obtained by FEKO (MoM) due to the limited computing power of commercial software.

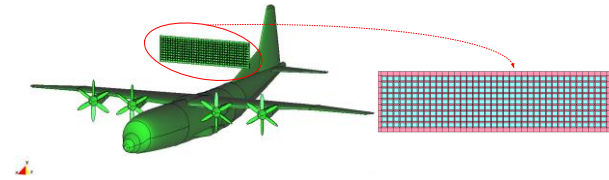


Fig. 12. Model of the four rotor aircraft mounting microstrip antenna array.

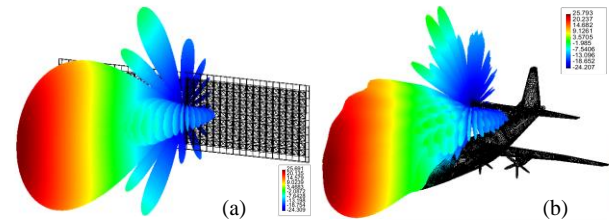


Fig. 13. Microstrip antenna array patterns: (a) array and (b) airborne array.

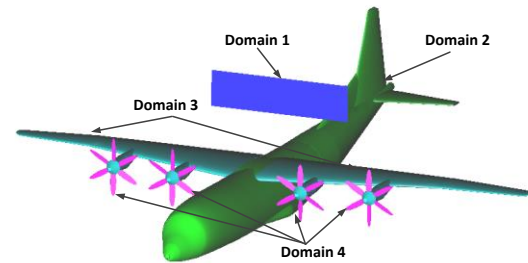


Fig. 14. Domain decomposition model (each color represents a subdomain).

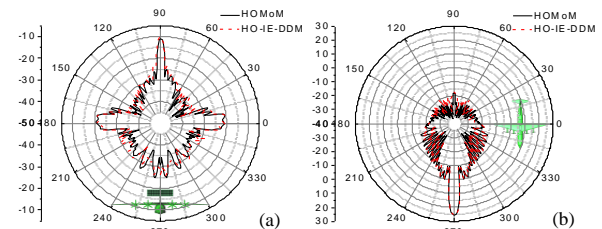


Fig. 15. 2D radiation patterns of the airborne microstrip array: (a) x-y and (b) x-z.

The computational statistics for solving each subdomain and entire problem are recorded in Table 3. It can be observed that the HO-IE-DDM leads to over 80% memory reduction compared with the overall solution for this example. Moreover, the speedup and parallel efficiency of the proposed parallel solver is evaluated

and shown in Fig. 16. The parallelized HO-IE-DDM performs well.

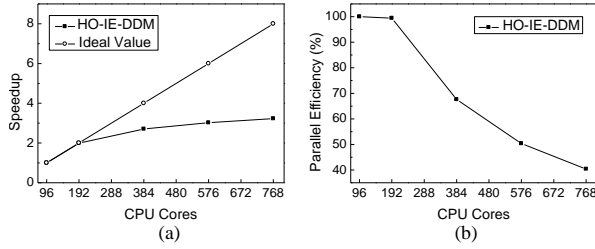


Fig. 16. Parallel performance of parallelized HO-IE-DDM for the airborne microstrip array: (a) speedup ratio and (b) parallel efficiency.

Table 3: Computational statistics of airborne microstrip array

| Method | Unknowns | Storage (GB) | Time (min) |
|------------------------|---------------------|---------------------|------------|
| HO-IE-DDM | 7568 (domain1) | 0.85 (domain1) | 259.14 |
| | 94692 (domain2) | 133.61 (domain2) | |
| | 110228 (domain3) | 181.05 (domain3) | |
| | 3648 (domain4) | 0.20 (domain4) | |
| HOMoM (out of core) | 250216 | 932.93 | 288.55 |

D. Airborne microstrip antenna array JEM characteristics

When airborne array is in an independent subdomain, the accuracy of the proposed method has been proved above. Based on quasi-stationary method, we calculate 360 rotor orientations of the four rotor wings in this example. In order to compare with modulation level, we spread the 3D radiation pattern of the rectangle patch microstrip array installed above a four-rotor aircraft along θ axis and ϕ axis in Fig. 17.

Table 4: Average modulation level (dB)

| Receive \ Transmit | Phi Polarized | Theta Polarized | Circularly Polarized |
|--------------------|----------------|-----------------|----------------------|
| | Yagi-Uda array | 52.01 | 50.73 |
| Microstrip array | 21.98 | 23.09 | 11.58 |

Similar to the last two-rotor aircraft case, JEM affects less in this four-rotor aircraft when the receiving antenna is circularly polarized. In Table 4, we can confirm this rule more intuitively from the data in the two cases. Figure 18 shows the changeable intensity of the airborne array radiation pattern at every observation

angles. Compared with Fig. 17 there also is a complementary relationship before and after the modulation. It shows that side-lobes and null depth levels of the airborne array are intensely changed.

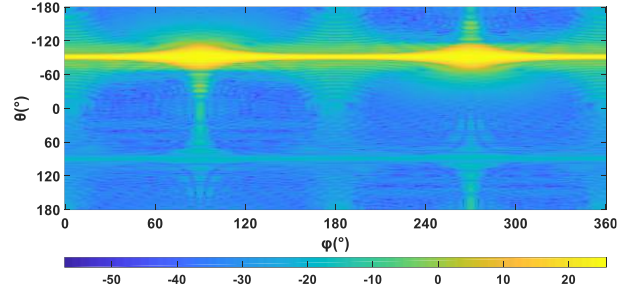


Fig. 17. Spreaded airborne microstrip array pattern.

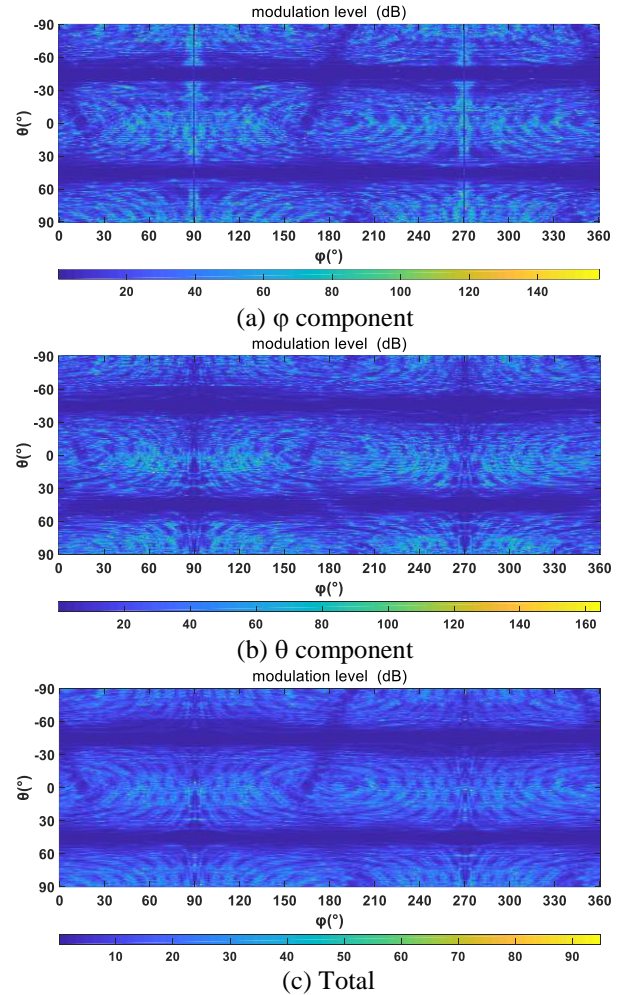


Fig. 18. Spreaded modulation level contour plots.

In Table 5, a comparison of the computational statistics between the HO-IE-DDM and HOMoM is shown. In the solution time, the computing time and the

iteration time for domain 4 is only 3.0 min totally. For the four rotor aircraft airborne antenna, the platform subdomains (domain 2-3) and the array part (domain 1) are unchanged and can be reused during the solution. Thus, the memory requirement and CPU time are greatly reduced. The proposed method is of great significance especially for the problems with changeable parts.

Table 5: Computational statistics of interfered microstrip array

| Method | Unknowns | Storage (GB) | Time (min) |
|-----------|-----------------------|-----------------------|---|
| HO-IE-DDM | 7568 (domain1) | 0.85 (domain1) | 254.5×1 (domain1-3) 3.0×360 (domain4) 1340.03 (total) |
| | 94692 (domain2) | 133.61 (domain2) | |
| | 110228 (domain3) | 181.05 (domain3) | |
| | 3648×360 (domain4) | 0.20×360 (domain4) | |
| HOMoM | 250216×360 | 932.93×360 | - |

IV. CONCLUSION

An efficient HO-IE-DDM algorithm is developed to solve large complex EMC problem, such as airborne array JEM interference problem. The proposed method provides unprecedented flexibility and convenience for the object with changeable parts, since it just needs to re-compute the changed parts of the model during the design process. The modulation level of a double rotor aircraft and a four rotor aircraft loading large antenna array respectively has been successfully obtained. Numerical results verify the feasibility and versatility of this method, and also reveal the radiation characteristics of airborne antennas affected by JEM effects.

ACKNOWLEDGMENT

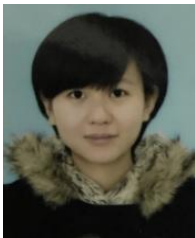
This work was supported in part by the National Key R&D Program of China under Grant 2017YFB0202102, in part by the China Postdoctoral Science Foundation funded project under Grant 2017M613068, in part by the National Key R&D Program of China under Grant 2016YFE0121600, and in part by the Special Program for Applied Research on Super Computation of the NSFC-Guangdong Joint Fund (the third phase) under Grant No. U150150.

REFERENCES

- [1] V. C. Chen, *The Micro-Doppler Effect in Radar*. USA: Artech House, 2011.
- [2] D. Gaglione, "MACHe-model-based algorithm for classification of helicopters," *IEEE A&E Systems Magazine*, vol. 1, pp. 38-40, 2016.
- [3] A. K. Singh and Y. H. Kim, "Automatic measurement of blade length and rotation rate of drone using W-band micro-Doppler radar," *IEEE Sensors Journal*, vol. 18, pp. 1895-1902, 2018.
- [4] T. Dogaru, K. Gallagher, and C. Le, "Doppler radar phenomenology in small commercial unmanned aerial systems," *U.S. Government Work*, pp. 205-206, 2017.
- [5] J. E. Richie and B. R. Koch, "The use of side-mounted loop antennas on platforms to obtain nearly omnidirectional radiation," *IEEE Trans. Antennas Propagat.*, vol. 53, pp. 3915-3919, 2005.
- [6] C. R. Birtcher, C. A. Balanis, and D. Decarlo, "Rotor-blade modulation on antenna amplitude pattern and polarization: Predictions and measurements," *IEEE Trans. EMC*, vol. 41, pp. 384-393, Nov. 1999.
- [7] Y. Zhang, T. K. Sarkar, and X. Zhao, *Higher Order Basis Based Integral Equation Solver (HOBBIES)*. Hoboken, New York: John Wiley, 2012.
- [8] Y. Li, X. Zhao, and H. Zhang, "Out-of-core solver based DDM for solving large airborne array," *Applied Computational Electromagnetics Society*, vol. 31, pp. 509-519, 2016.
- [9] Z. Peng, X. C. Wang, and J. F. Lee, "Integral equation based domain decomposition method for solving electromagnetic wave scattering from non-penetrable objects," *IEEE Trans. Antennas and Propag.*, vol. 59, pp. 3328-3338, 2011.
- [10] W. Li, W. Hong, and H. Zhou, "An IE-ODDM-MLFMA scheme with DILU preconditioner for analysis of electromagnetic scattering from large complex objects," *IEEE Trans. Antennas and Propag.*, vol. 56, pp. 1368-1380, 2008.
- [11] L. Guo, Y. Chen, J. Hu, and R. Zhao, "A novel JMCIE-DDM for analysis of EM scattering and radiation by composite objects," *IEEE Antennas and Wireless Propag. Letters*, vol. 16, pp. 389-392, 2017.
- [12] Y. Zhang and T. K. Sarkar, *Parallel Solution of Integral Equation Based EM Problems in the Frequency Domain*. John Wiley & Sons, Hoboken, NJ, USA, 2009.
- [13] Y. Wang, X. Zhao, Y. Zhang, S. W. Ting, T. K. Sarkar, and C. H. Liang, "Higher order MoM analysis of traveling-wave waveguide antennas with matched waveports," *IEEE Trans. Antennas and Propag.*, vol. 63, pp. 3718-3721, 2015.
- [14] Z. Lin, Y. Chen, and Y. Zhang, "Study of the parallel higher-order MoM on a domestically-made CPU platform," *Journal of Xidian University (Natural Science)*, vol. 3, pp. 43-47, 2015.
- [15] Q. Su, Y. Liu, and X. Zhao, "Parallel integral equation-based nonoverlapping DDM for solving challenging electromagnetic scattering problems of two thousand wavelengths," *International Journal of Antennas and Propagation*, 2019.
- [16] Z. Peng and B. M. Mason, "High-performance surface integral equation solvers towards extreme-scale electromagnetic modeling and simulation,"

Proceedings of the 2016 IEEE/ACES International Conference on Wireless Information Technology and Systems and Applied Computational Electromagnetics, pp. 1-2, 2016.

- [17] SP Ltd, "NATOPS Flight Manual: Navy Model E-2C Plus Aircraft," US Navy: Navair 01-E2AAB-1, 1999.
- [18] V. Pan'ko, Y. Salomatov, and V. Ovechkin, "Software for designing of dipole antenna arrays, multi-frequency matching with wide band antennas," *Proceedings of the IEEE-Russia Conference*, vol. 4, pp. 36-38, 1999.



Yingyu Liu received the B.S. degrees from Xidian University, Xi'an, China, in 2013. Her current research interests include high performance electromagnetic computing based on supercomputer platforms.



Qin Su received the B.S. degree from Xidian University, Xi'an, China, in 2012, and is currently working toward the Ph.D. degree at Xidian University. His current research interests is computational electromagnetic.



Xunwang Zhao received the B.S., and Ph.D. degrees from Xidian University, Xi'an, China, in 2004, and 2008, respectively. He joined Xidian University as a Faculty Member in 2008. As Principal Investigator, he is doing or has completed some projects including project of NSFC.